

Self-assembly of strongly dipolar molecules on metal surfaces

Donna A. Kunkel, James Hooper, Scott Simpson, Daniel P. Miller, Lucie Routaboul, Pierre Braunstein, Bernard Doudin, Sumit Beniwal, Peter Dowben, Ralph Skomski, Eva Zurek, and Axel Enders

Citation: *The Journal of Chemical Physics* **142**, 101921 (2015); doi: 10.1063/1.4907943

View online: <http://dx.doi.org/10.1063/1.4907943>

View Table of Contents: <http://scitation.aip.org/content/aip/journal/jcp/142/10?ver=pdfcov>

Published by the [AIP Publishing](#)

Articles you may be interested in

[Temperature-dependent self-assembly of NC-Ph₅-CN molecules on Cu\(111\)](#)

J. Chem. Phys. **142**, 101928 (2015); 10.1063/1.4909518

[Solution-growth kinetics and thermodynamics of nanoporous self-assembled molecular monolayers](#)

J. Chem. Phys. **134**, 124702 (2011); 10.1063/1.3569132

[Self-assembly of semifluorinated n -alkanethiols on {111}-oriented Au investigated with scanning tunneling microscopy experiment and theory](#)

J. Chem. Phys. **127**, 024702 (2007); 10.1063/1.2746252

[Following transformation in self-assembled alkanethiol monolayers on Au\(111\) by in situ scanning tunneling microscopy](#)

J. Chem. Phys. **115**, 6672 (2001); 10.1063/1.1403000

[The role of dimer formation in the self-assemblies of DNA base molecules on Cu\(111\) surfaces: A scanning tunneling microscope study](#)

J. Chem. Phys. **115**, 3419 (2001); 10.1063/1.1384551



Computing
SCIENCE & ENGINEERING

AIP'S JOURNAL OF COMPUTATIONAL TOOLS AND METHODS.
AVAILABLE AT MOST LIBRARIES.

Self-assembly of strongly dipolar molecules on metal surfaces

Donna A. Kunkel,¹ James Hooper,² Scott Simpson,^{3,4} Daniel P. Miller,³ Lucie Routaboul,⁵ Pierre Braunstein,⁵ Bernard Doudin,⁶ Sumit Beniwal,¹ Peter Dowben,¹ Ralph Skomski,¹ Eva Zurek,^{3,a)} and Axel Enders^{1,b)}

¹Department of Physics, University of Nebraska-Lincoln, Lincoln, Nebraska 68588, USA

²Department of Theoretical Chemistry, Faculty of Chemistry, Jagiellonian University, 30-060 Krakow, Poland

³Department of Chemistry, 331 Natural Sciences Complex, Buffalo, New York 14260, USA

⁴School of Science, Penn State Erie, The Behrend College, 28 Hammermill, Erie, Pennsylvania 16563, USA

⁵Lab de Chimie de Coordination, Institut de Chimie (UMR 7177 CNRS), Université de Strasbourg, 67081 Strasbourg, France

⁶Institut de Physique et Chimie des Matériaux de Strasbourg (IPCMS UMR 7504 CNRS) and Lab of Nanostructures in Interactions with their Environment (NIE), Université de Strasbourg, 23 Rue du Loess, 67034 Strasbourg, France

(Received 5 December 2014; accepted 30 January 2015; published online 24 February 2015)

The role of dipole-dipole interactions in the self-assembly of dipolar organic molecules on surfaces is investigated. As a model system, strongly dipolar model molecules, *p*-benzoquinonemonoimine zwitterions (ZI) of type $C_6H_2(\cdots NHR)_2(\cdots O)_2$ on crystalline coinage metal surfaces were investigated with scanning tunneling microscopy and first principles calculations. Depending on the substrate, the molecules assemble into small clusters, nano gratings, and stripes, as well as in two-dimensional islands. The alignment of the molecular dipoles in those assemblies only rarely assumes the lowest electrostatic energy configuration. Based on calculations of the electrostatic energy for various experimentally observed molecular arrangements and under consideration of computed dipole moments of adsorbed molecules, the electrostatic energy minimization is ruled out as the driving force in the self-assembly. The structures observed are mainly the result of a competition between chemical interactions and substrate effects. The substrate's role in the self-assembly is to (i) reduce and realign the molecular dipole through charge donation and back donation involving both the molecular HOMO and LUMO, (ii) dictate the epitaxial orientation of the adsorbates, specifically so on Cu(111), and (iii) inhibit attractive forces between neighboring chains in the system ZI/Cu(111), which results in regularly spaced molecular gratings. © 2015 AIP Publishing LLC. [<http://dx.doi.org/10.1063/1.4907943>]

I. INTRODUCTION

In the context of the self-assembly of organic molecular adsorbates on surfaces, which is currently a very active area of research, the role of molecular dipoles is frequently discussed [see for instance other articles in this Special Topic on supramolecular self-assembly, or the themed collection: Ref. 26]. A number of studies have suggested that the intermolecular dipole-dipole interaction might play a significant role in how molecules are aligned within supramolecular assemblies. In some cases, these interactions were shown to dominate over forces resulting from chemical bonds between the molecules. Various examples can be found in published studies of organics under ambient atmospheric conditions,¹ at the liquid-solid interface² and under ultrahigh vacuum conditions,³⁻⁸ with the molecular dipole aligned perpendicular to the surface⁹ or within the surface plane,^{3,4} and for various molecule sizes ranging from small molecules such as quinonoid zwitterions³ and styrenes⁴ to larger ones such as anthracene.¹⁰ In reviewing those reported assemblies of dipolar molecules, it becomes evident that most of them do

not correspond to a configuration of lowest electrostatic energy. Instead, molecules of similar dipole moment can repel each other on one surface⁹ and attract each other on another.¹¹ Molecules were observed to arrange their dipoles into linear chains,⁷ one-dimensional chains of alternating dipole orientation,³ rings,⁸ domains of parallel dipole alignment,⁴ porous two-dimensional (2D) networks with 90° dipole alignment,⁷ and honeycomb networks of more complex moment alignment.¹² Multiple phases were often observed on the same sample.^{13,14} One would expect, however, that if dipolar interactions were indeed driving the molecular self-assembly then only one final configuration, one that represents the electrostatic minimum, would be observed for dipolar molecules. As is evident from the brief review above, this is clearly not the case.

This study systematically investigates how a small set of model dipolar molecules adsorb on various metal surfaces in both experiment and theory; the goal is to elucidate the role of the intrinsic molecular dipole during self-assembly. We select a recently discovered class of molecules with unusually strong intrinsic dipoles as a model system, which are the *p*-benzoquinonemonoimine zwitterions (ZI), $C_6H_2(\cdots NHR)_2(\cdots O)_2$.^{15,16} Molecules with R=H (Figures 1(a) and 1(b)) are considered as the parent molecule (PZI) of an entire family. Numerous derivatives have been prepared

^{a)}Electronic mail: ezurek@buffalo.edu

^{b)}Electronic mail: aenders2@unl.edu

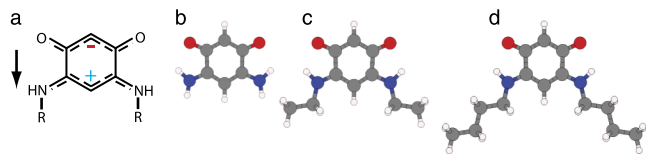


FIG. 1. Chemical structure (a) and the DFT optimized geometries of the quinonoid zwitterion molecules used for this study. (b) PZI, (c) EZI, and (d) BZI. The arrow in (a) indicates the direction of the intrinsic dipole. Color code: oxygen—red, carbon—grey, nitrogen—blue, and hydrogen—white.

with other R substituents. We selected ethyl zwitterions (EZI, where $R=C_2H_5$) and butyl zwitterions (BZI, where $R=C_4H_9$), in addition to the smaller PZI for this study (see Figure 1). The electrically neutral molecules carry positive and negative charges on opposite parts of the molecule, the positive charge being delocalized between the nitrogen functions over four bonds involving 6π -electrons, while the negative charge is likewise spread between the oxygen atoms. We will refer to the anionic trimethylene oxonol moiety of the molecule ($O\cdots C\cdots CH\cdots C\cdots O$) as the top part or anionic part of the molecule and to the trimethylene cyanine part ($HRN\cdots C\cdots CH\cdots C\cdots NHR$) as the bottom part or cationic part in this paper. Both cationic and anionic parts give the molecules a large electric dipole moment of approximately 10 Debye (D) or 3.33×10^{-29} C m.¹⁵

In the crystalline state, the dipoles of neighboring molecules tend to point in opposite directions, thus effectively canceling out the dipole and reducing the electrostatic energies.^{15–18} This structure is thought to be driven by strong molecular dipoles, together with $NH\cdots OH$ -bond formation between adjacent molecules. Under UHV conditions on the (111) faces of the coinage metals Ag, Au, and Cu, molecule-substrate interactions play a deterministic role in what self-assembled structures quinonoid zwitterions form.^{3,19}

An important consideration in this discussion is that the dipole moment of a molecule adsorbed onto a metal substrate deviates, often drastically, from the dipole moment of a free molecule. In an earlier study, we have reported that the magnitude of the dipole moment of a ZI molecule adsorbed to an Ag or Cu cluster (a finite model for the substrate-adsorbate system) yields a dipole moment that is approximately one sixth of the free molecule value or approximately 1.5 D.³ This change in dipole results from a substrate-mediated charge exchange between the HOMO and the LUMO of the molecules. But the opposite is also observed: styrene molecules are nearly non-polar as free molecules but acquire a significant in-plane dipole when adsorbed to Ag(100) but not on Ag(111).⁸ Similarly, 4-fluorostyrene, which possesses a dipole moment as a free molecule, has a moment that is twice as large on Cu(111) and Au(111).⁵ Another example is tetrathiafulvalene (TTF) which acquires a considerable dipole moment out of the film plane of nearly 5 D on Au(111).²⁰

In this paper, we will analyze several factors that contribute to the self-assembly of ZI on metal surfaces, including chemical bond formation, epitaxial considerations, dipolar interactions, and substrate-mediated long-range interactions. We will show that the structure formation on surfaces is mainly

driven by a competition between intermolecular interactions and molecule-substrate interactions. Dipolar interactions are determined to be too small to be significant by comparison, despite the considerable gas-phase dipole moment of the ZI.

II. EXPERIMENTAL METHODS

The experimental investigation was performed in ultra-high vacuum at a base pressure of 1×10^{-10} millibars. Metal substrates, such as Ag(111), Au(111), and Cu(111), were prepared *in-situ* by repeated cycles of Ar ion sputtering and subsequent annealing at approximately 600 °C. The cleanliness of the surfaces was checked with scanning tunneling microscopy (STM). Characteristic for the clean Au(111) surface is the so-called herringbone reconstruction, which is described in earlier publications, including in the article by Murphy *et al.* in this Special Topic. This reconstruction is seen easily in STM images of the Au surface in this article. The molecules were synthesized as described in Refs. 15, 16, and 18. In the vacuum system, the molecules were thermally evaporated from a Knudsen cell onto the substrates, which were held at room temperature during film growth. The deposition rate was about 0.03–0.5 monolayers per minute, depending on the desired coverage. After deposition, the samples were transferred *in-situ* into an Omicron low-temperature STM where they were imaged at a temperature of 77 K. The STM was operated with electrochemically etched tungsten tips. Coverages are quoted in monolayers (ML) throughout this paper. However, the definition of a monolayer is difficult to make for this system, given the broad range of different structures and packing densities observed. We refer to coverage as the estimated percentage of substrate surface covered, ignoring actual packing densities of the molecules.

III. COMPUTATIONAL METHODS

Density Functional Theory (DFT) calculations (geometry optimizations, electronic densities of states, and charge densities) were performed using the Vienna *Ab-initio* Simulation Package (VASP) version 5.3.5.²¹ The projector augmented wave (PAW) method²² was used to treat the core states along with a plane-wave energy cutoff of 500 eV, and the C/N/O $2s/2p$, H $1s$, Cu $4s/3d$, Ag $5s/4d$, and Au $6s/5d$ electrons were treated explicitly. The Perdew-Burke-Ernzerhof (PBE) functional²³ and its revised formulation (revPBE)²⁴ were used along with post-SCF dispersion corrections from the 3rd generation, “Grimme3,” of Grimme’s corrections (DFT-D3).²⁵

The Γ -centered Monkhorst-Pack scheme was used to generate k -point grids for each system, and the energies were converged such that the difference between the ones provided in the manuscript and those calculated with larger grids were (typically much) less than 0.03 eV/molecule. A Γ -point grid was sufficient to achieve convergence for isolated molecular networks. The copper, silver, and gold surfaces were constructed from the experimental face-centered cubic lattice constant of 3.615, 4.086, and 4.078 Å for

Cu, Ag, and Au, respectively. Each surface was simulated using a four layer thick slab; the top two layers of the slab were allowed to relax during geometry optimizations, while the bottom two were kept fixed to the experimental lattice constant. A dipole correction, as implemented with the LDIPOL tag in VASP, was applied along the direction perpendicular to the metal surface, or the z -axis, in all calculations. A vacuum space of at least 15 Å (10 Å for the molecular networks in the absence of metal slabs) ensured that there would be no interaction between periodic images of the slab in the z -direction. The “free” zwitterion was optimized in a box measuring $(25 \times 25 \times 25)$ Å and the dipole correction was applied to all directions of the simulation cell.

IV. EXPERIMENTAL RESULTS

We begin our analysis of the self-assembly of dipolar molecules by comparing the growth of PZI's on the surfaces of Ag(111), Au(111), and Cu(111) at sub-monolayer coverage. The STM images presented in Figure 2, which we discussed in-part in Refs. 3 and 19, reveal key differences in how the same molecules bind together in order to form a condensed phase.

On Ag(111) and Au(111), the PZI typically form islands where the two NH₂ groups of each molecule bind to the O-groups of two neighboring molecules via hydrogen bonds, thus creating a 2D network that exhibits a nearly square-shaped unit cell. From this bonding scheme follows parallel alignment of the dipolar molecules so that the islands must exhibit remnant non-zero electric polarization. Boundaries between structural domains of opposite molecular orientation are frequently observed. Differences between the PZI islands on Au and Ag are in the outer shape of the islands and the epitaxial relationship to the substrate. By contrast, the PZI assemble into one-dimensional chains on Cu(111), as seen in Figure 2(c). Within those chains, each PZI forms 4 H-bonds with its neighbors. Each molecule binds to 2 other molecules in a chain and to 4 other molecules in the 2D islands. The alternating orientation of the molecules along a 1D chain apparently cancels the in-plane component of the net dipole moment.

This finding of substrate-dependent bonding schemes of the PZI is remarkable and raises the question as to what is actually the determining factor during the self-assembly. In this section, we will present additional experimental results and further investigate the role of the molecular R-groups.

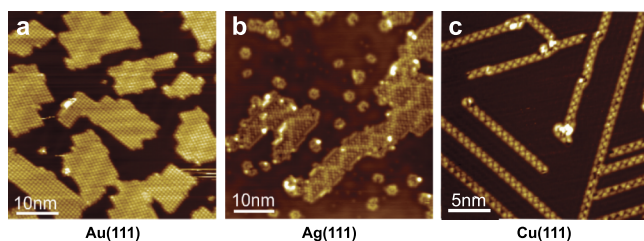


FIG. 2. STM images of parent zwitterions on three different substrate surfaces, Au(111) (a), Ag(111) (b), and Cu(111) (c).

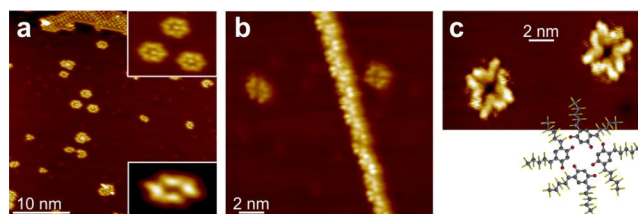


FIG. 3. STM images showing quinonoid zwitterion molecules on Ag(111). (a) Parent zwitterions, (b) ethyl zwitterions, and (c) butyl zwitterions. A structure model of a BZI tetramer is shown in (c).

A. Ring-shaped clusters of zwitterions

First, we want to focus on an interesting structure, small ring-like clusters of the ZI, visible in Figure 2(b). Such clusters are occasionally observed on both Ag and Au substrates at sub-monolayer coverage, albeit with much higher frequency on Ag(111). Interestingly, similar clusters were never observed on Cu(111). Molecular rings are also formed by the EZI and the BZI on Ag(111), as the STM images in Figure 3 show. PZI were observed to form clusters with a distribution of sizes where heptamers, PZI₇, appear to be most frequent. Two selected characteristic clusters, a tetramer and a heptamer, are highlighted in Figure 3(a). Both EZI and BZI form almost exclusively tetramers.

The size of the molecule, specifically the length of the R-groups, increases from PZI to EZI and BZI. The STM images resolve the molecular structure sufficiently so that the location of the R-groups of the molecules is clearly visible. It is therefore evident that the particular arrangement of the molecules in a tetramer is the result of the molecules pointing “inward” to the center of the cluster, so that they can form H-bonds with one another within geometrical constraints provided by the R-groups. This is particularly clear in the BZI tetramers in Figure 3(c). As the structure model in the figure shows, the formation of a H-bond with each neighbor in this ring-like arrangement creates a characteristic offset bond angle between the molecules, which is clearly seen in the STM image. The geometrical constraint by the R-groups likely limits the cluster size. We assume that the same bonding scheme is also present in the tetramers of EZI and PZI. For PZI, however, the geometrical constraints due to the functional groups is considerably smaller, so that also larger rings of molecules, typically consisting of 6 molecules per ring, are not only possible but also most frequently observed. Zoomed-in images suggest that those rings also have a seventh molecule in the inside, resulting in heptamers. Given the significantly smaller size of the PZI, we were unable to determine the exact alignment of the central molecule.

B. Chains and gratings of parent zwitterions

Here, we are concerned with assemblies of the PZI on Cu(111). STM images of the PZI on Cu(111) at various sub-monolayer coverages are shown in Figures 2(c) and 4. The bonding scheme of the 1D chains of molecules has already been discussed earlier in this section, and more extensively in Ref. 3. Signature features of the chains are the 4 hydrogen bonds the molecules form with 2 neighbors, as well as the

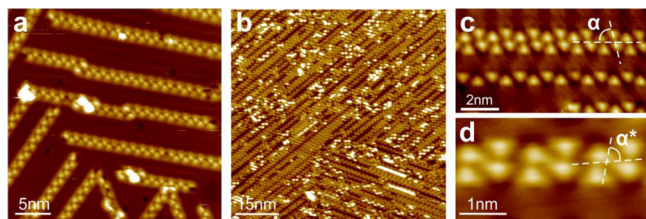


FIG. 4. ((a) and (b)) STM images of parent zwitterion molecules on Cu(111) at two different sub-monolayer coverages. ((c) and (d)) Magnified images of selected PZI chains showing details of the stacking of neighboring chains at higher coverage. $U_{bias} = +0.3$ V; $+0.75$ V; -0.2 V and -0.75 V in (a)-(d), respectively.

alternating molecular orientation perpendicular to the chain axis. The same alternating arrangement has been observed for ZI on HOPG after preparation in solution² and in the bulk crystalline form.^{15–17} In both cases, it had been concluded that this arrangement, where gas phase dipole moments would effectively cancel each other, is partly due to electrostatic energy minimization.

The study of the PZI on Cu(111) as a function of coverage in the sub-monolayer regime shows that the 1D chains appear to stay separated from one another at very low coverage, indicating repulsive chain-chain interactions. The repulsive nature of the interaction is also evident from STM images of EZI and BZI on the same substrate, which will be discussed in Sec. IV C. Close inspection of the STM image in Figure 4(a) reveals characteristic standing wave patterns in the electron density within the substrate surface, which is a well-known phenomena related to the Shockley surface state electrons of the Cu(111) surface.²⁷ Electronic surface states, especially the Shockley state of the Cu(111) surface, have been shown to critically influence the molecular self-assembly.²⁸ Their role in this present system will be discussed in more detail in Sec. V.

At higher coverage, above 0.5 ML of adsorbed PZI, repulsive chain interactions appear to be less dominant as neighboring chains are now observed to be close, see Figures 4(b)-4(d). The high-magnification STM images show details of how molecules are aligned within the chains and how chains bind together, and also give us clues about how the molecules interact with the substrate. Each molecule appears as a triangle in the STM images where the pointy end of the triangle corresponds to the anionic oxygen functions of the molecules. The alternating molecule alignment within the chains is thus clearly visible.

The molecular zigzag chains stack up such that each molecule in one chain has a direct neighbor in the adjacent chain that is of the same orientation. As a result, columns of molecules of the same orientation are formed nearly perpendicular to the chain axes due to chain stacking. More precisely, these columns form an angle of $\alpha = 78^\circ \pm 5^\circ$ with respect to the chain direction as indicated in the STM image 4(c) and 4(d). The shift occurs with two different orientations, i.e., bonding to the left or right, both of which are commonly observed.

It is further observed from image 4(c) that the electron density in the Cu substrate directly under the anionic oxygen functions is reduced, visible as darker contrast in the image,

while the electron density in the Cu substrate directly under the cationic nitrogen functions is increased, visible as brighter contrast.

C. Chains and gratings of ethyl and butyl zwitterions

An overview over experimental results of the growth of EZI on the three substrates Au(111), Ag(111), and Cu(111) for two coverages in the sub-monolayer regime is provided in Figure 5. Likewise, STM images showing BZI on the same substrates are presented in Figure 6. Unlike the parent zwitterions, which form 2D islands on Ag and Au, the BZI form linear chains on all three substrates. Also, the EZI are typically observed to form linear chains, although we have reported 2D island formation in an earlier study.³ The reason for 1D chain formation is simple: hydrogen bond formation involves the oxygen- and amine groups of the molecules, and for EZI and BZI, this is only possible for alternating molecular orientation due to the constraining R groups. A 2D bonding scheme, where all molecules point in the same direction, is only possible with the NHR groups if $R=H$.¹⁹

A number of interesting observations can be made from a comparison of the STM images of the EZI and BZI chains on the three surfaces. First, both the EZI chains and the BZI chains follow the herringbone reconstruction of the Au(111) surface, without lifting the reconstruction. Only if the coverage approaches a full monolayer, the chains straighten out by overcoming the substrate's template effect. Second, for the EZI and BZI, the chain-chain interactions also seem to be repulsive on Cu(111), as seen from the almost perfectly equidistant separation of the chains, especially in the case of EZI. Bunching of the chains, i.e., overcoming of the repulsive forces, is again observed only as the coverage approaches the monolayer limit. This is especially visible in the shown high-coverage image for BZI.

Our STM study showed that there are significant differences in how the 1D chains of the ZI stack together within the surface plane at higher coverage. Differences are evident between the molecule types as well as the substrates they are on, see Figures 4 and 7. The stacking of rows of PZI on Cu(111) into columns of molecules has already been discussed. The stacking of the BZI molecular chains, by

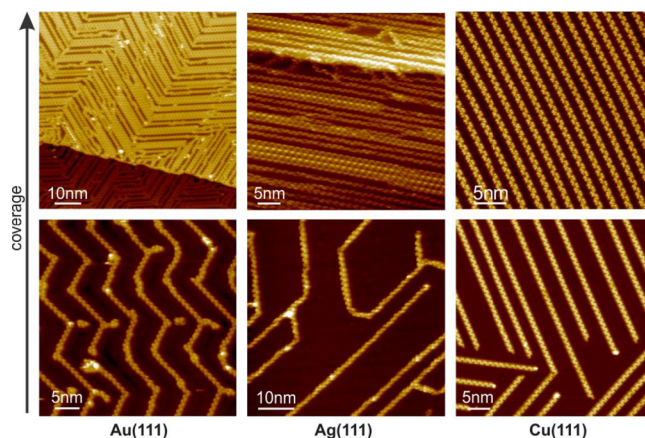


FIG. 5. Representative STM images of ethyl zwitterion molecules on the (111) surfaces of Au, Ag, and Cu, for two different sub-monolayer coverages.

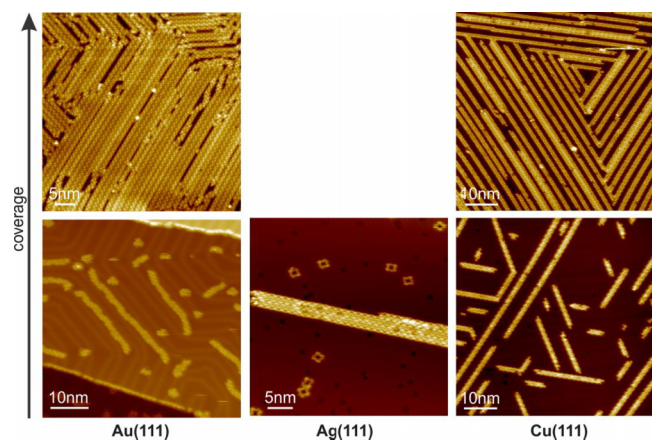


FIG. 6. Representative STM images of butyl zwitterion molecules on the (111) surfaces of Au, Ag, and Cu, for two different sub-monolayer coverages.

contrast, is reminiscent of a lock-and-key mechanism resulting from the V-shaped arrangement of the butyl groups. The stacking of EZI chains is substrate-dependent: EZI molecules bind back-to-back in neighboring chains on Ag, have the lock-and-key arrangement like the BZI's on Cu, and have an intermediate arrangement on the Au surface.

V. DISCUSSION

A. Calculated structure models and epitaxial considerations

To better understand the supramolecular forces that guide their formation, dispersion-corrected density functional theory (DFT-D3) calculations were carried out for the two networks of PZI that form on Cu(111) and Ag(111)/Au(111). Gas-phase models were built of: (1) the network in which the molecular dipole moments of each adsorbate are aligned, the “2D” electret network shown in Figure 8(a), and (2) a close-packed sheet built from the “1D” zigzag chains discussed above, shown in Figure 8(b). The structures were optimized in different-sized cells, without a metallic substrate, to find their optimal gas phase geometries. When each network was constrained to lie in a plane, the 2D electret network was found to be the lowest in energy by approximately 0.23 eV/molecule. When fully relaxed without the planar constraint, the electret network remained more-or-less flat but the ZI molecules that make up the zigzag chains tilted so that the chains could be pushed closer together. This results in the energy of the zigzag network being reduced by 0.15 eV/molecule, which is still insufficient to overcome the energy of the electret structure. Thus, it could be expected that the 2D electret network should form if the interactions between the PZI and the substrate are not strong enough to offset the energetic preference of the 2D network, as is likely the case from the STM studies of Ag(111) and Au(111).

The most apparent quantitative difference in the intermolecular bonding is the shorter hydrogen bond distance in the 2D network, which measures ~ 1.70 Å vs. ~ 1.85 Å in the zigzag network. This suggests that the lower energy of the 2D networks is, at least in part, a result of the increased strength

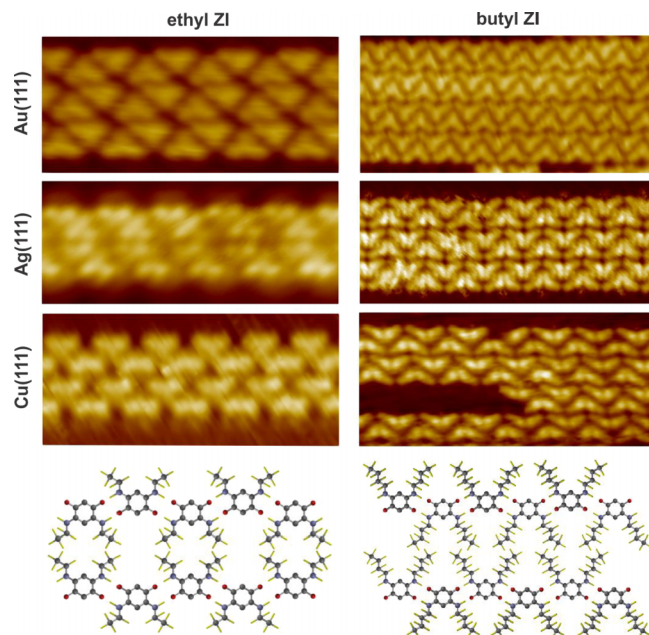


FIG. 7. STM images showing details of the stacking of neighboring chains of EZI (left) and BZI (right), on the substrates as indicated. Bottom: structure models of EZI on Ag(111) and of BZI on all substrates.

of the hydrogen bonds. Inspection of the electrostatic potential around a PZI molecule, on an electron density isosurface with a 0.01 a.u. isovalue (see Figure 8(c)), confirms that its local (and global) minimum around the oxygen atoms coincides with the position where the hydrogen bond in the 2D network is found. Furthermore, the energy of an isolated molecule whose

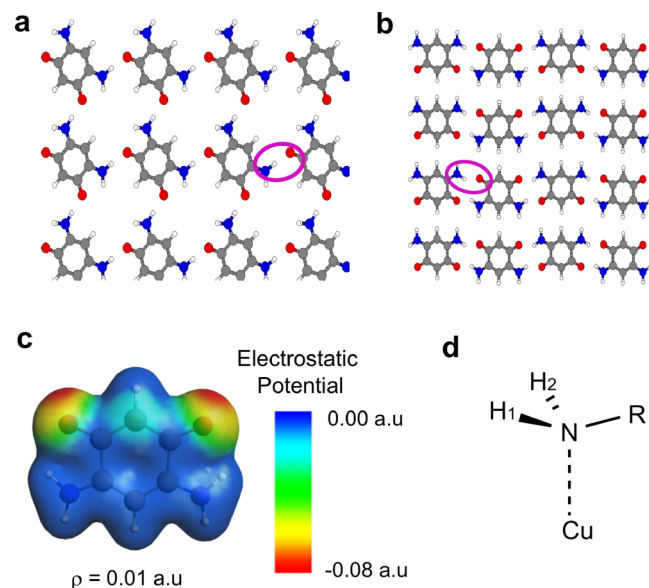


FIG. 8. The DFT-D3 optimized geometries of (a) the PZI with aligned dipole moments to form the 2D “electret” network and (b) the PZI with alternating dipole moments similar to the observed zigzag 1D chains. Circles highlight the relative orientation of the atoms comprising the hydrogen bond. (c) The electronic charge density of an isolated gas phase PZI (isovalue 0.01 a.u.) colored by the electrostatic potential. Note that the hydrogen atom involved in a hydrogen bond in (a) points towards the red region, whereas the one in (b) points towards the yellowish region. (d) A sketch of the local geometry around the N atom when PZI is adsorbed to Cu(111).

atomic coordinates were extracted directly from each extended network showed that the molecular constituents of the 2D networks were 0.16 eV/molecule lower in energy than those of the zigzag network. The most notable geometric difference between the structures of the two monomers is the shortest distance between the oxygen atom and a hydrogen atom in the amine group; the $O \cdots H$ distance measures 2.08 Å in the electret and 2.39 Å in the zigzag networks. This suggests that the intramolecular hydrogen bonding interactions are greater in the electret structure, and this could be why the individual molecules are more stable. Although the molecular dipole-dipole and dispersion interactions, among others, contribute to the differences in energies, we believe the hydrogen bond strengths are the most important factors determining the energy difference between the two networks.

To analyze how the isolated PZI molecules interact with the substrate, the binding energy (BE) was computed via

$$BE = E_{\text{surf-ads}} - E_{\text{surface}} - E_{\text{ads}}, \quad (1)$$

where $E_{\text{surf-ads}}$ is the energy of the molecule optimized on its respective surface, E_{surface} is the energy of the periodic metal slab, and the third term is the energy of an isolated PZI molecule. The BE was the largest on the Cu surface (−1.88 eV), followed by Au (−1.40 eV) and Ag (−1.23 eV). Thus, the 0.23 eV/molecule energy difference between planar networks is, in itself, quite small when compared with the computed BE of the PZI to any of the substrates.

The corrugation of the potential energy surface (PES) across the Au(111) surfaces is small, 0.04 eV on Au.¹⁹ In fact, studies of benzene on various metal surfaces have also shown that the variations in the PES with the different adsorption sites, top (T), bridge (B), and hollow (H), is fairly small, on the order of a few tens of meV.^{19,29–33} This not only implies that the diffusion barrier is low but it also means that the molecules are not strictly pinned to particular adsorption sites on the surface.

On Cu(111), however, the corrugation energy of the PES of the PZI is calculated to be at least ~0.47 eV, more than ten times larger than that of silver and gold (see the supplementary material³⁵) and double the difference between the planar 2D and 1D gas-phase networks. The lowest-energy binding site considered in this study placed the nitrogen atoms on top of a copper atom (T-site) and the oxygen atoms over a H_{fcc} site (see the supplementary material³⁵). The interaction between the Cu and N has an impact on the geometry around the nitrogen atom, which is sketched in Figure 8(d). The Cu—N distance measures 2.15 Å and the hydrogen atoms pucker away from the surface so that the hybridization of the nitrogen atom appears to change from sp^2 to sp^3 upon adsorption; the Cu—N—H₁, Cu—N—H₂, and Cu—N—R angles measure 109.4°, 106.6°, and 101.1°, respectively. Other systems with this type of $RH_2Cu \cdots N$ interaction have previously been synthesized in, for example, a Cu complex with benzene-1,2-diamine ligands, wherein the Cu—N distances measure roughly 2.0 Å.³⁴ The orientation required to place both amine groups on top sites forces them to align along a crystallographic high-symmetry direction on the Cu(111) surface, which again agrees with how the 1D chains were characterized from experiment, as seen for instance in Figure 2.

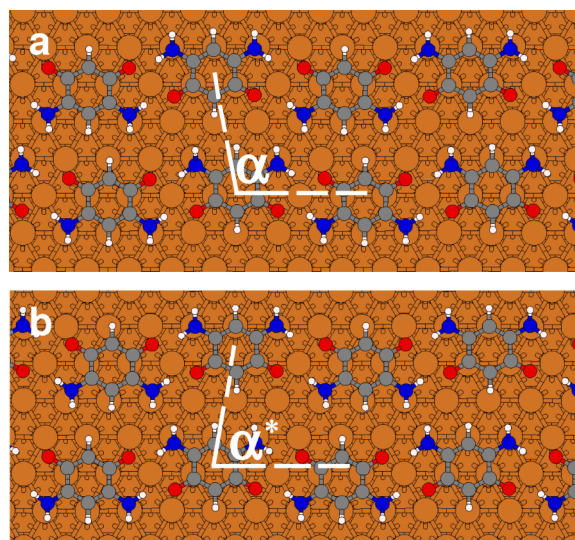


FIG. 9. Model of the PZI double chains on Cu(111). Since the epitaxial fit is likely driven by the strong site preference of the N atoms of the molecule, the models were built to ensure that all of the N atoms are situated near T sites. The chain offset angles α and α^* are a result of the epitaxial fit.

The geometry optimizations of an isolated PZI molecule adsorbed to Cu(111) on various binding sites (see the supplementary material³⁵) provide support for the argument that the binding of the N atom to Cu is primarily responsible for the strong epitaxy observed on the Cu surface. Furthermore, a surface model can easily be built using experimental distances, which constructs extended zigzag chains while placing each nitrogen over a top site; a model of two such PZI chains stacked beside each other is shown in Figure 9 and is supported by two findings from experiment: (i) the molecular chains align along 3 distinct (high-symmetry) directions on the surface (Figure 2(c)) and (ii) the placement of the amine groups of the molecules in the zigzag chains at top sites creates a slight shift of one chain vs. the other, which is clearly seen in the STM images, such as Figure 4.

The energy of an isolated (gas-phase) zigzag chain constrained to the simplest, rectangular, two-molecule simulation cell that is required to align the nitrogen atoms in the NH_2 groups over top sites of the Cu(111) surface is roughly 0.5 eV/molecule higher than the energy of the optimized (gas-phase) 2D network geometry. Since this difference is comparable to the corrugation energy of ZI on Cu(111), it is not obvious that the zigzag chain is energetically preferred on the surface. Therefore, models of the 2D electret network, as shown in the supplementary material,³⁵ were constructed over a Cu(111) slab. The models were built by searching for cells of a Cu(111) slab that matched up best with the optimized parameters of the 2D PZI network. The BE of the model zigzag network was lower than any of the electret configurations that were considered. It is noted that the energy difference is sensitive to the functional that was employed, as described in the supplementary material,³⁵ but even the electret model with the lowest binding energy, computed with the PBE-D3 functional, was found to have a binding energy that is 0.05 eV/molecule less negative than the zigzag model. Thus, the computations are in agreement with experiment: the zigzag

network is energetically preferred over the electret structure on the Cu(111) surface. Moreover, because the electret network is preferred in the gas phase, it is likely to have a lower energy on substrates that have little corrugations in the PES, such as Au(111).

Additional computational details and additional results of the functional group position analysis, along with structure coordinates, are provided in the supplementary material.³⁵

B. Analysis of the dipole-dipole interaction

One of the central questions in organic self-assembly, which has motivated this study, is about the role of the molecular dipole moment. For a pair of two dipoles, \vec{p}_1 and \vec{p}_2 , the dipole-dipole interaction energy is dependent on the separation distance, \vec{r} , and the relative orientation of the dipoles and given by

$$U = \frac{1}{8\pi\epsilon_0} \frac{1}{r^3} [\vec{p}_1 \cdot \vec{p}_2 - 3(\vec{p}_1 \cdot \hat{r})(\vec{p}_2 \cdot \hat{r})]. \quad (2)$$

However, this expression assumes that the separation distance is large compared to the dipole length itself. This assumption is typically not correct in self-assembled monolayers where molecular dipoles are close-packed. Hence, for correct evaluation, each dipole has to be considered as assumed opposite Coulombic point charges, separated by a distance that corresponds to the dipole length. The electrostatic energy follows from summation over each pair of charges:

$$U = \frac{1}{8\pi\epsilon_0} \sum_{i=1}^n \sum_{j=1}^n \frac{q_i q_j}{r_{ij}}, \quad (3)$$

where r_{ij} is the distance connecting the i th and j th charges. We have evaluated the electrostatic energies for the experimentally observed structures of the PZI using expression (3). The actual dipole moments of the adsorbed PZI, calculated with DFT in a previous study,³ were used. Calculations showed that on all three metals the net dipole of the substrate-adsorbate system assumes a canted out-of-plane direction. Here, only the component of the dipole moments parallel to the substrate surface and the measured experimental dipole separations were used to estimate the energy of three configurations: molecules all aligned into electret domains, single alternating chains, and multiple alternating chains. The calculated in-plane dipole components are given in Table I.

The magnitude of the out of plane dipole moments do not vary significantly for the three systems studied: 1.2 D, 1.1 D, and 1.3 D for Au, Ag, and Cu, respectively.³ Therefore, the interaction energy of the out of plane components of the dipole moments should be comparable on the three surfaces and effectively raises the total interaction energy in a similar fashion for all configurations studied. Thus, out-of-plane components of the dipoles were omitted in the following; our estimate represents a lower limit.

Table I displays the calculated dipolar energies of the configurations under consideration. Experimentally determined distances were used when available. When not available, a reasonable estimate was used. As can be seen, the energies per molecule vary from -0.1 to -4 meV. These calculated energies need to be compared to typical

TABLE I. Dipolar energies per molecule of adsorbed parent quinonoid zwitterions. The dipole shown corresponds to the in-plane component of the total dipole of the adsorbate-substrate system.

Energy/Mol. (meV)	Geometry	Dipole (D)	Substrate
-1	Single chain	0.89	Au(111)
-3	Multichain	0.89	Au(111)
-2	Diamond	0.89	Au(111)
-2	Single chain	1.1	Ag(111)
-4	Multichain	1.1	Ag(111)
-2	Diamond	1.1	Ag(111)
-0.1	Single chain	0.3	Cu(111)
-0.5	Multichain	0.3	Cu(111)
-0.1	Diamond	0.3	Cu(111)

energies of H-bonds (170-650 meV),³⁶ van der Waals bonds (<50 meV),³⁷ CH— π bonds (60–100 meV),³⁸ π — π bonds (100 meV),³⁸ and metal-ligand bonds (500–2000 meV).³⁸ For an additional comparison, the difference in bonding site energies for adsorbed ZI on the Au(111) surface was reported to be 40 meV,¹⁹ which by itself was declared inconsequentially small. A similar assessment of the role of dipolar interactions has been made by Talapin *et al.*, which considered inorganic nanoparticles with an extremely large dipole moment of 100 D (which is an order of magnitude larger than any organic molecule) and a radius of 5.8 nm.³⁹ Even in such an extreme case, the dipolar energy was only -39 meV/particle, which is still significantly less than a hydrogen bond energy. This analysis suggests that the dipole energy is unlikely the governing factor in organic self-assembly.

C. Long-range surface-mediated interactions

Other substrate effects include the scattering of surface state electrons, which causes the charge density waves visible in Figure 4(a). Also, the screening of the localized charge in the molecules by the substrate electrons, visible in Figure 4(c), is a well-known interface effect. Both scattering and screening of charge can cause long-range Friedel-type oscillatory interactions between the adsorbates, which can be attractive or repulsive depending on the adsorbate spacing.^{40,41} Earlier studies have already demonstrated that metallic substrates can indeed mediate long-range interactions and influence atomic and molecular ordering. Examples include shells of atoms,⁴¹ zwitterionic nano gratings,⁴² the self-aligned atomic strings in bimolecular gratings,⁴³ and porous networks of anthraquinone molecules.⁴⁴ Reported energies for substrate-mediated interactions are of the order of one or more milli electron volts over a distance of a few nanometers (see overview in Ref. 40 and references therein) so that the resulting structures are typically observed at low temperatures.

We believe that the observed repulsive interaction between the molecular chains is substrate-mediated, and specifically the result of charge redistribution (pillow effect) in the proximity of the contact area between adsorbates and substrate.^{45-47,50} Such a redistribution of electronic charge around adsorbates on coinage metal surfaces has been shown experimentally in several studies,^{19,28,48} and is actually visible in the STM images in Figures 4(c) and 4(d). This mechanism

is often found to be more pronounced on Cu(111) than on Ag(111) or Au(111). For instance, tetraphenylporphyrin molecules, 2H-TPP, were observed to experience attractive intermolecular forces on Ag(111), but repulsive interactions on Cu(111) due to the charge pillow effect.⁴⁹ This is consistent with the formation of ZI nano gratings on Cu(111) in this study.

VI. SUMMARY

The study of the self-assembly of small molecules with a strong intrinsic dipole moment on the single crystal surfaces of various coinage metals has been instructive to evaluate the driving forces during structure formation generally and to test the role of the dipole-dipole interaction specifically. Quinonoid zwitterions with 3 types of functional groups (hydrogen, ethyl, and butyl groups) have been investigated on Ag(111), Au(111), and Cu(111) as model systems.

Given the significant structural differences between the observed assemblies, it is clear that dipole-dipole interactions cannot be the outstanding dominant mechanism during self-assembly in all cases. Instead, our analysis has shown that there is rather a hierarchy of attractive and repulsive intermolecular interactions of different strengths, including H-bonding, dipolar interactions, charge transfer, screening, pillow effect, and epitaxial alignment of the adsorbate to the substrate. Electrostatic energies were found to be small compared to other energies and thus can only play a secondary role. Such a complex interplay of forces, however, has resulted in a variety of different structures, such as islands, rings, and gratings of molecules, and the substrate turns out to be an important parameter to control the growth of organic nanostructures.

Our DFT calculations confirm that the 2D electret configuration is energetically preferred over the zigzag bonding scheme in the gas phase and on substrates where the binding energy to the substrate and the site specificity is weak, such as Au and Ag. On Cu, however, the considerably stronger site specificity of the NH₂ groups favored the zigzag bonding scheme over the electret. The difference in bonding scheme of the PZI—electret on Au and Ag versus zigzag chains on Cu—is thus ascribed to differences in binding energy of the molecules between the substrates, specifically to the particularly strong locking of the molecular nitrogen atoms to the top sites of the Cu surface. Besides this mechanism, there is repulsion between the chains of all ZI on the Cu surface due to the charge pillow induced in the Cu around the direct contact area, resulting in nano gratings.

The significance of this study is thus in the analysis of the role of molecular dipoles in the context of other interactions during self-assembly and how they modify the intrinsic surface dipole of metal surfaces, which is expected to impact the current discussion of the self-assembly of organics on surfaces.

ACKNOWLEDGMENTS

The authors acknowledge support from the National Science Foundation through the Materials Research Science and Engineering Center (Grant No. DMR-1420645) and

through NSF Grant No. EPS-1004094. J.H. acknowledges financial support from the Homing Plus Program (HOMING PLUS/2012-6/4) granted by the Foundation for Polish Science and co-financed by the European Regional Development Fund. We acknowledge support from the Center of Computational Research at SUNY Buffalo. E.Z. thanks the Alfred P. Sloan Foundation for a Research Fellowship (2013-2015).

- ¹J. N. Hohman, P. Zhang, E. I. Morin, P. Han, M. Kim, A. R. Kurland, P. D. McClanahan, V. P. Balema, and P. S. Weiss, *ACS Nano* **3**, 527 (2009).
- ²Y. Fang, P. Nguyen, O. Ivasenko, M. P. Aviles, E. Kebede, M. Askari, X. Ottenwaelder, U. Ziener, O. Siri, and L. Cuccia, *Chem. Commun.* **47**, 11255 (2011).
- ³D. A. Kunkel, S. Simpson, J. Nitz, G. A. Rojas, L. Routaboul, P. Braunstein, B. Doudin, P. A. Dowben, E. Zurek, and A. Enders, *Chem. Comm.* **48**, 7143 (2012).
- ⁴A. Baber, S. Jensen, and E. Sykes, *J. Am. Chem. Soc.* **129**, 6368 (2007).
- ⁵A. D. Jewell, S. Simpson, A. Enders, E. Zurek, and E. C. H. Sykes, *Phys. Chem. Lett.* **3**, 2069 (2012).
- ⁶K. R. Harikumar, T. Lim, I. McNab, J. C. Polanyi, L. Zotti, S. Ayissi, and W. A. Hofer, *Nat. Nanotechnol.* **3**, 222 (2008).
- ⁷S. Kuck, S.-H. Chang, J.-P. Klöckner, M. H. Proscenc, G. Hoffmann, and R. Wiesendanger, *ChemPhysChem* **10**, 2008 (2009).
- ⁸O. Vaughan, A. Alavi, F. Williams, and R. Lambert, *Angew. Chem., Int. Ed.* **47**, 2422 (2008).
- ⁹T. Yokoyama, T. Takahashi, K. Shinozaki, and M. Okamoto, *Phys. Rev. Lett.* **98**, 206102 (2007).
- ¹⁰Y. Wei, W. Tong, and M. B. Zimmt, *J. Am. Chem. Soc.* **130**, 3399 (2008).
- ¹¹T. Bauert, L. Zoppi, G. Koller, A. Garcia, K. K. Baldrige, and K.-H. Ernst, *J. Phys. Chem. Lett.* **2**, 2805 (2011).
- ¹²Z. Mu, Q. Shao, J. Ye, Z. Zeng, Y. Zhao, H. H. Hng, F. Boey, J. Wu, and X. Chen, *Langmuir* **27**, 1314 (2011).
- ¹³W. Tong, X. Wei, and M. B. Zimmt, *J. Phys. Chem. C* **113**, 17104 (2009).
- ¹⁴W. Tong, Y. Wei, K. W. Armbrust, and M. B. Zimmt, *Langmuir* **25**, 2913 (2009).
- ¹⁵O. Siri and P. Braunstein, *Chem. Commun.* **2002**, 208.
- ¹⁶P. Braunstein, O. Siri, J. Taquet, M.-M. Rohmer, M. Bénard, and R. Welter, *J. Am. Chem. Soc.* **125**, 12246 (2003).
- ¹⁷F. Tamboura, C. Cazin, R. Pattacini, and P. Braunstein, *Eur. J. Org. Chem.* **2009**, 3340.
- ¹⁸Q.-Z. Yang, O. Siri, and P. Braunstein, *Chem. Eur. J.* **11**, 7237 (2005).
- ¹⁹S. Simpson, D. A. Kunkel, J. Hooper, J. Nitz, P. A. Dowben, L. Routaboul, P. Braunstein, B. Doudin, A. Enders, and E. Zurek, *J. Phys. Chem. C* **117**, 16406 (2013).
- ²⁰I. Fernandez-Torrente, S. Monturet, K. J. Franke, J. Fraxedas, N. Lorente, and J. I. Pascual, *Phys. Rev. Lett.* **99**, 176103 (2007).
- ²¹G. Kresse and J. Hafner, *Phys. Rev. B* **47**, 558 (1993).
- ²²P. Blöchl, *Phys. Rev. B* **50**, 17953 (1994).
- ²³J. P. Perdew, K. Burke, and M. Ernzerhof, *Phys. Rev. Lett.* **77**, 3865 (1996).
- ²⁴Y. Zhang and W. Yang, *Phys. Rev. Lett.* **80**, 890 (1998).
- ²⁵S. Grimme, J. Antony, S. Ehrlich, and H. Krieg, *J. Chem. Phys.* **132**, 154104 (2010).
- ²⁶“Scanning probe studies of molecular systems,” guest editors S. De Feyter, N. Lin, and Steven Tait, *Chem. Commun.*, 2014 (entire volume).
- ²⁷M. F. Crommie, C. P. Lutz, and D. M. Eigler, *Nature* **363**, 524 (1993).
- ²⁸G. Rojas, S. Simpson, X. Chen, D. A. Kunkel, J. Nitz, J. Xiao, P. A. Dowben, E. Zurek, and A. Enders, *Phys. Chem. Chem. Phys.* **14**, 4971 (2012).
- ²⁹W. Liu, J. Carrasco, B. Santra, A. Michaelides, M. Scheffler, and A. Tkatchenko, *Phys. Rev. B* **86**, 245405 (2012).
- ³⁰D. Miller, S. Simpson, N. Tyminńska, and E. Zurek, *J. Chem. Phys.* **142**, 101924 (2015).
- ³¹J. Carrasco, W. Liu, A. Michaelides, and A. Tkatchenko, *J. Chem. Phys.* **140**, 084704 (2014).
- ³²T. S. Chwee and M. B. Sullivan, *J. Chem. Phys.* **137**, 134703 (2012).
- ³³A. Bilić, J. R. Reimers, N. S. Hush, R. C. Hoft, and M. J. Ford, *J. Chem. Theory Comput.* **2**, 1093 (2006).
- ³⁴S. Supriya and S. K. Das, *Inorg. Chem. Commun.* **6**, 10 (2003).
- ³⁵See supplementary material at <http://dx.doi.org/10.1063/1.4907943> for additional computational details.

- ³⁶T. Steiner, *Angew. Chem., Int. Ed.* **41**, 48 (2002).
- ³⁷L. Xu, X. Miao, X. Ying, and W. Deng, *J. Phys. Chem. C* **116**, 1061 (2011).
- ³⁸G. A. Rojas, "Self assembly and interface chemistry of non-metallated tetraphenyl porphyrin," Ph.D. thesis (University of Nebraska, Lincoln, 2011).
- ³⁹D. V. Talapin, E. V. Shevchenko, C. B. Murray, A. V. Titov, and P. Král, *Nano Lett.* **7**, 1213 (2007).
- ⁴⁰A. Enders, R. Skomski, and J. Honolka, *J. Phys.: Condens. Matter* **22**, 433001 (2010).
- ⁴¹V. S. Stepanyuk, N. N. Negulyaev, L. Niebergall, and P. Bruno, *New J. Phys.* **9**, 388 (2007).
- ⁴²A. Schiffrin, A. Riemann, W. Auwarter, Y. Pennec, A. Weber-Bargioni, D. Cvetko, A. Cossaro, A. Morgante, and J. V. Barth, *Proc. Natl. Acad. Sci. U. S. A.* **104**, 5279 (2007).
- ⁴³A. Schiffrin, J. Reichert, W. Auwärter, G. Jahnz, Y. Pennec, A. Weber-Bargioni, V. Stepanyuk, L. Niebergall, P. Bruno, and J. Barth, *Phys. Rev. B* **78**, 1 (2008).
- ⁴⁴G. Pawin, K. L. Wong, K.-Y. Kwon, and L. Bartels, *Science* **313**, 961 (2006).
- ⁴⁵P. Bagus, K. Hermann, and C. Woll, *J. Chem. Phys.* **123**, 184109 (2005).
- ⁴⁶P. Bagus, V. Staemmler, and C. Wöll, *Phys. Rev. Lett.* **89**, 096104 (2002).
- ⁴⁷H. Vasquez, Y. Dappe, J. Ortega, and F. Flores, *Appl. Surf. Sci.* **254**, 378 (2007).
- ⁴⁸L. Vitali, G. Levita, R. Ohmann, A. Comisso, A. D. Vita, and K. Kern, *Nat. Mater.* **9**, 320 (2010).
- ⁴⁹G. Rojas, X. Chen, C. Bravo, J.-H. Kim, J.-S. Kim, J. Xiao, P. A. Dowben, Y. Gao, X. C. Zeng, W. Choe, and A. Enders, *J. Phys. Chem. C* **114**, 9408 (2010).
- ⁵⁰S. Simpson and E. Zurek, *J. Phys. Chem. C* **116**, 12636 (2012).